PHYSICAL REVIEW B **84**, 220103(R) (2011)

Pentavacancy as the key nucleus for vacancy clustering in aluminum

Hao Wang,[1,2,*] David Rodney,[1] Dongsheng Xu,[2] Rui Yang,[2] and Patrick Veyssière[3,†]
[1]*Science et Ingénierie des Matériaux et Procédés (SIMAP), Institut Polytechnique de Grenoble, CNRS/Université Joseph Fourier, Boîte Postale 46, F-38402 Saint Martin d'Hères, France*
[2]*Institute of Metal Research, Chinese Academy of Sciences, Shenyang 110016, China*
[3]*Laboratoire d'Etude des Microstructures (LEM), CNRS/Office National d'Etudes et de Recherches Aérospatiales (ONERA), Boîte Postale 72, F-92322 Châtillon, France*
(Received 5 November 2011; published 12 December 2011)

The atomic-scale process of vacancy clustering, of fundamental importance in conditions of quenching, irradiation, and plastic deformation, is studied in aluminum. Clustering is known to lead to large crystalline defects such as dislocation loops, but the early stages of the process are still largely unknown. Using a combination of molecular dynamics simulations, the activation-relaxation technique and kinetic Monte Carlo simulations, a specific cluster, containing five vacancies and forming a local body-centered-cubic cell in the face-centered-cubic lattice, is found to play a crucial role. It is revealed that this cluster of very high stability is the nucleus for the growth of larger clusters during annealing of quenched supersaturated samples.

DOI: 10.1103/PhysRevB.84.220103 PACS number(s): 61.72.Cc, 61.72.jd, 61.72.Bb

Vacancies are fundamental to the kinetics of metals because of their role in atomic diffusion.[1] When produced in supersaturation, for instance, during quenching,[2] irradiation,[3] or plastic deformation,[4] vacancies cluster to form secondary defects, such as dislocation loops, that strongly affect the metal properties and in particular its resistance to plastic deformation.[5] The process of vacancy clustering has been studied in details in body-centered-cubic (bcc) metals by means of multiscale modeling.[6,7] By contrast, the situation in face-centered-cubic (fcc) metals is far less clear. In aluminum of specific interest here, it is known from electrical resistivity measurements[8] and positron annihilation spectroscopy (PAS)[8,9] that vacancy clustering starts above 200 K and that large clusters in the form of dislocation loops are visible in electron microscopy above room temperature.[10] But in the intermediate temperature range, the so-called stage III, the defect clusters are too small to be identified. PAS (Ref. 9) showed that the microstructure contains a specific type of defect clusters in addition to monovacancies, but the nature of this cluster, as well as its possible role as nucleus for the growth of larger loops, is still unknown.

To clarify the microscopic processes at the origin of vacancy clustering in fcc metals, we started by studying a specific case of vacancy supersaturation. Molecular dynamics (MD) simulations with embedded atom method (EAM) potentials are employed to simulate the time evolution of the vacancy supersaturation produced inside narrow edge dislocation dipoles, i.e., close pairs of edge dislocations with opposite Burgers vectors, of the type that form under plastic deformation (details of the simulation can be found in Ref. 11). An example of simulation in aluminum at a temperature close to the melting temperature is shown in Fig. 1(a). At such elevated temperatures, the vacancies diffuse along the dipole and form a large number of a specific cluster, noted as V_5. This cluster contains five vacancies and will be called a *pentavacancy*. As shown in Fig. 1(b), pentavacancies consist of six vacancies replacing the atoms at the six face centers of a fcc unit cell with an interstitial atom at the center of the cell, thus forming a bcc unit cell in the fcc crystal. Other appearances of this cluster can be found, e.g., in Fig. 6 of Ref. 12, in Fig. 5 of Ref. 11, and in Fig. 12 of Ref. 13, although the cluster structure was not identified at that time. The pentavacancy is mentioned in early theoretical studies of vacancy clusters[14,15] but its possible role in vacancy clustering has not been considered so far.

The stability and energy of pentavacancies are studied by molecular statics employing several EAM interatomic potentials and *ab initio* electronic structure calculations based on the density functional theory. Aluminum is special in the sense that in this metal, the pentavacancy is of high stability compared to other clusters. *Ab initio* calculations yield a formation energy of 2.32 eV, compared to $5 \times 0.67 = 3.35$ eV for five isolated vacancies. Locally, the bcc unit cell has a lattice parameter of 3.32 Å, resulting in an elastic contraction of the surrounding fcc lattice, whose equilibrium parameter is 4.05 Å. For this calculation, a periodic supercell with $3 \times 3 \times 3$ fcc unit cells was used within the projected augmented-wave method and generalized gradient approximation of Perdew-Burke-Ernzerhof. We used a cutoff energy of 300 eV, a Methfessel-Paxton smearing of 1 eV, and a Monkhorst-Pack k-point mesh of $15 \times 15 \times 15$.

The stability of pentavacancies compared to other vacancy clusters was further confirmed in aluminum by computing the binding energy of mono- and divacancies to clusters containing from $N = 1$ to 8 vacancies. The binding energy is defined as $E_f(N) + E_f(m) - E_f(N+m)$,[6] where $E_f(N)$ is the formation energy of a cluster containing N vacancies and $m = 1$ and 2 for mono- and divacancies, respectively. Figure 2(a) shows the result obtained with the aluminum EAM potential of Mishin *et al.*[16] and *ab initio* calculations. For each cluster size, only the conformation of the lowest formation energy (hereafter denoted V_N) is considered and presented in the insets of Fig. 2(a). There is a good agreement between EAM potential and *ab initio* calculations, with very large binding energies of both V_1 and V_2 to V_5, which is due to the low formation energy of V_5. This energy is in fact so large that the binding energies of V_1 to V_6 and V_2 to V_7 are negative.

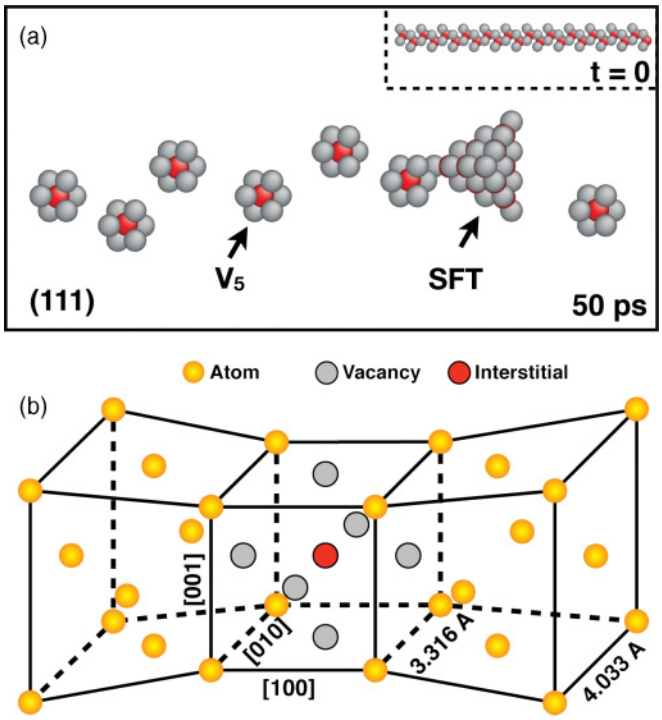

FIG. 1. (Color online) (a) Annihilation of an edge dislocation dipole at high temperature in Al leading to the formation of pentavacancies after 50 ps (the inset shows the initial configuration). (b) Schematic representation of the local lattice around a pentavacancy. Spheres represent vacancies, interstitials, and filled fcc sites as indicated on the figure.

We show below that the pentavacancy plays a central role in the early stage of vacancy clustering in aluminum. This process was studied experimentally by finite-time annealing treatments of quenched samples at temperatures between 200 and 400 K.[2,8,17] We simulated this out-of-equilibrium process using the kinetic Monte Carlo (KMC) method parametrized on atomistic calculations. Reproducing all recovery stages observed experimentally is very difficult because it requires to account both for complex phenomena such as the transition between vacancy clusters and dislocation loops, and for the sample microstructure, particularly the density of vacancy sinks, which depends on the grain size. Our aim here is to account quantitatively for the first stage of vacancy recovery, called stage III, which involves only small clusters, too small to be visible in electron microscopy. We thus computed the input parameters for the KMC simulation, i.e., the activation energies for migration, absorption, and dissociation, for clusters up to seven vacancies and employed for larger clusters phenomenological extrapolations. The latter affect the high-temperature recovery stages (particularly stage IV), but we checked that they do not alter the stage III of interest here. Given the large amount of calculations to be performed, we employed the EAM potential of Mishin *et al.*. The potential energy landscape of the clusters was explored using the activation-relaxation technique (ART), a single-ended eigenvector-following method (see Ref. 18 and references therein). As in the work of Marinica *et al.*[19] for interstitial clusters in bcc iron, ART found a great variety of thermally activated paths and cluster configurations spreading a large energy range. The case of five-vacancy clusters is shown in Fig. 3, which confirms that the pentavacancy configuration is a well-defined energy minimum, with a formation energy 0.8 eV lower than all other five-vacancy clusters and separated from the latter by energy barriers larger than 0.8 eV. Among all transitions, we identified those corresponding to migration, dissociation, and absorption of the clusters. Table I lists the activation energies for absorption and dissociation. As an example, the two energy barriers circled in Fig. 3 and illustrated by the insets correspond to the absorption of a monovacancy by a tetravacancy (0.24 eV) and a divacancy by a trivacancy (0.23 eV). Both reactions lead to a pentavacancy, respectively 0.87 and 0.98 eV lower in energy. In agreement with Table I, the activation energy for absorption $V_4 + V_1 \rightarrow V_5$ (respectively $V_3 + V_2 \rightarrow V_5$) is thus 0.24 eV (respectively 0.23 eV) and for the reverse dissociation reaction, $0.24 + 0.87 = 1.11$ eV (respectively $0.23 + 0.98 = 1.21$ eV).

For migration, ART found single-step paths for clusters up to five vacancies, i.e., paths with a single energy barrier. V_2 has the lowest migration energy (0.295 eV) followed by V_3 (0.600 eV), which is close to V_1 (0.635 eV) and lower than V_4 (0.660 eV). The lowest migration path for V_5 involves a collective motion of atoms with a single energy barrier of 1.22 eV. V_5 can thus migrate but only at high temperatures. Clusters larger than V_5 have multistep migration paths with activation energies much larger than 1 eV and, as a result, their migration was not included in the KMC simulations.

Absorption and dissociation paths for clusters from V_1 to V_7 are shown in Fig. 2(b) along with schematic representations of the atomic rearrangements involved with V_1. For each transition, only the lowest-energy path (reconstructed using the nudged elastic band method[20]) is shown. The discontinuities in the figure are due to the (elastic) interaction between the incoming vacancy and the existing cluster before absorption. Activation energies for absorption (respectively dissociation) are the difference between maximum and initial energies along the paths when the cluster size increases (respectively decreases). Paths with V_2 are included as they are often involved in cluster growth due to the high V_2 mobility. Absorptions by clusters smaller than V_5 decrease the energy, reflecting the positive binding energies shown in Fig. 2(a). Growing to V_6 increases slightly the energy, consistent with the negative binding energy of V_1 to V_6 in Fig. 2(a). Larger than V_7, the absorption energy is approximated by the V_1 migration energy and the dissociation energy by the V_1 migration energy plus the binding energy approximated with the $N^{2/3}$ classical phenomenological binding law for voids.[21]

The KMC simulations are based on the residence time algorithm,[22] with a classical attempt frequency of 10^{13} s^{-1} for all events. A cubic simulation cell containing $80 \times 80 \times 80$ fcc unit cells is used with periodic boundary conditions. Each cluster occupies a lattice site. Migration and dissociation may occur toward any first-neighbor site that does not already contain a cluster. If a first-neighbor site contains a cluster, absorption of the smaller cluster is included in the event list. Absorbing boundary conditions are applied along one face of the simulation cell to account for the presence of vacancy sinks. Each simulation starts with a random distribution of V_1, with concentrations between 10^{-4} and 10^{-3}, representative of the vacancy supersaturation produced in rapidly quenched

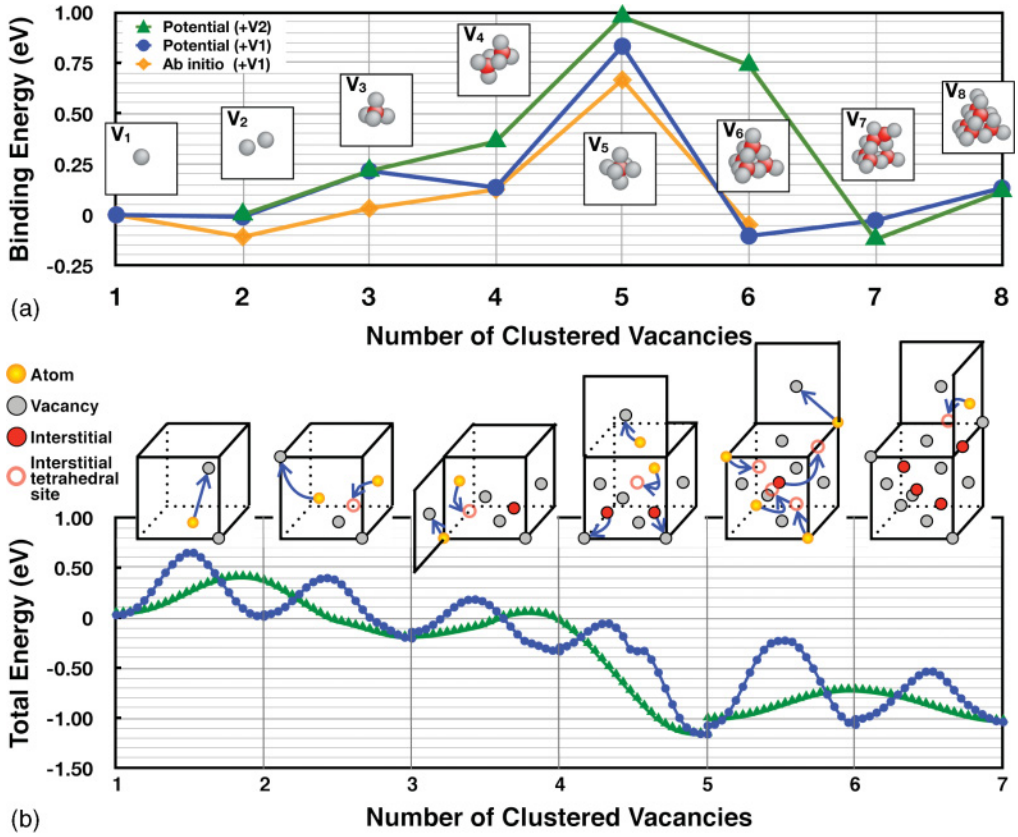

FIG. 2. (Color online) Energetics of vacancy clustering in aluminum. (a) Binding energy of mono- and divacancies to the most stable clusters containing from $N = 1$ to 8 vacancies (see the text for definition). The energies are computed using an EAM potential (Ref. 16) for monovacancies ($m = 1$, circles) and divacancies ($m = 2$, triangles), and with *ab initio* calculations for monovacancies (diamonds). Vacancy and interstitial configurations in the clusters are shown in the insets. (b) Evolution of the energy during the clustering of seven vacancies from isolated vacancies (taken as a reference energy) to the lowest-energy configuration of a seven-vacancy cluster. Absorption of monovacancies (circles) and divacancies (triangles) are shown. The absorption processes of monovacancies are shown schematically above the paths.

aluminum.[23] Annealing is then simulated at constant temperature for 2000 s to correspond to experimental conditions.[8] Figures 4(a) and 4(b) show the time evolution of the vacancy distribution per cluster size at two different temperatures for an initial concentration of 5×10^{-4} and Fig. 4(c) shows the density of clusters at various sizes as a function of temperature at the end of the annealing. Clusters containing six or more vacancies are treated together (denoted V_L in Fig. 4).

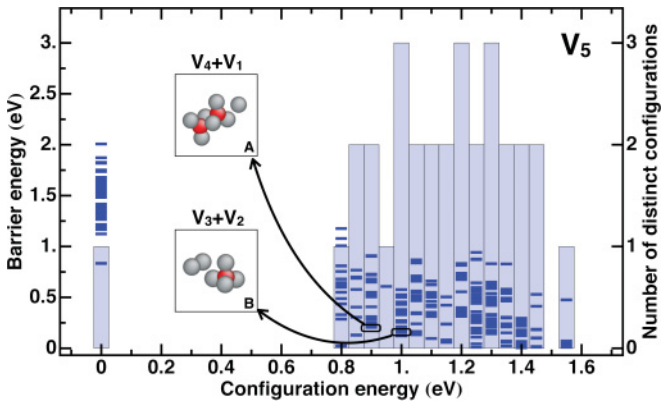

FIG. 3. (Color online) Histogram of formation and barrier energies for clusters of five vacancies. Cluster formation energies (with a bin size of 0.05 eV) are shown against the activation energies of transitions that transform the clusters (dashes with an energy scale on the left-hand-side). The pentavacancy formation energy is used as a reference. The number of distinct configurations for each formation energy is given by the bars associated with the right-hand-side scale.

TABLE I. Activation energies (E_{act}) and energy differences (ΔE) for the dissociation and absorption of clusters containing up to seven vacancies. Columns on the left correspond to dissociations, and on the right to absorptions. For V_6 and V_7, transitions involving V_3 have activation energies larger than 2 eV and are thus not included.

ΔE (eV)	E_{act} (eV)	$\longleftrightarrow$	E_{act} (eV)	ΔE (eV)
0.01	0.63	$V_1 + V_1 \leftrightarrow V_2$	0.62	−0.01
0.24	0.60	$V_2 + V_1 \leftrightarrow V_3$	0.36	−0.24
0.19	0.52	$V_3 + V_1 \leftrightarrow V_4$	0.33	−0.19
0.49	0.88	$V_2 + V_2 \leftrightarrow V_4$	0.39	−0.49
0.87	1.11	$V_4 + V_1 \leftrightarrow V_5$	0.24	−0.87
0.98	1.21	$V_3 + V_2 \leftrightarrow V_5$	0.23	−0.98
−0.01	0.90	$V_5 + V_1 \leftrightarrow V_6$	0.91	0.01
0.71	1.10	$V_4 + V_2 \leftrightarrow V_6$	0.39	−0.71
0.03	0.45	$V_6 + V_1 \leftrightarrow V_7$	0.42	−0.03
0.02	0.28	$V_5 + V_2 \leftrightarrow V_7$	0.26	−0.02

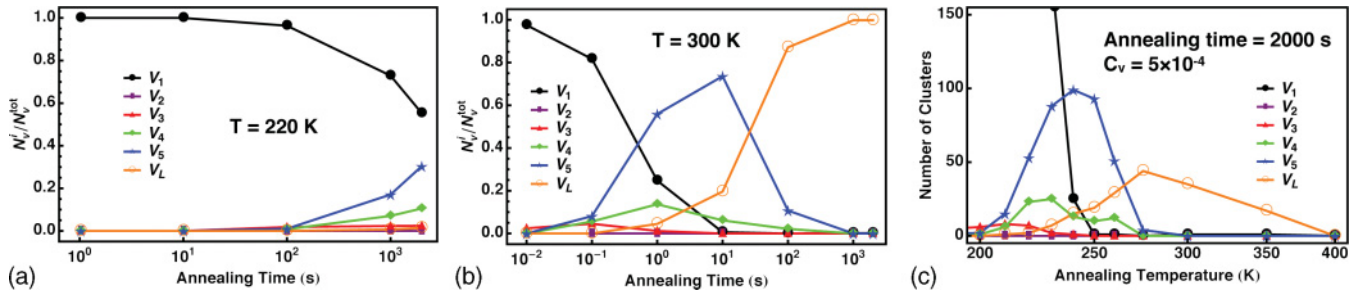

FIG. 4. (Color online) Vacancy clustering during annealing. (a) and (b) Distribution of vacancies in clusters with respect to annealing time at 220 K (stage III) and 300 K (stage IV), respectively. (c) Distribution of clusters after annealing with respect to annealing temperature. N_v^i is the number of vacancies in clusters of size i, and N_v^{tot} the total number of vacancies. V_L refers to clusters larger than V_5.

The KMC simulations reveal that pentavacancies are the dominant defect cluster in the temperature range between ∼200 and 250 K, which was identified experimentally as stage III,[8,9] and serve as nuclei for larger clusters at higher temperature, in stage IV. In agreement with experiments, clustering starts at 200 K and V_2 is responsible for most of the diffusion because of its high mobility. Below 200 K, the vacancies are not mobile enough to form clusters within the annealing time. The typical scenario is that two V_1 join to form one V_2, which migrates rapidly through the cell until it absorbs another vacancy, forming a V_3. The latter has a similar mobility as V_1 and migrates until it absorbs a vacancy, forming a V_4 of both lower mobility and stability (its dissociation energy is only 0.36 eV). The V_4 remains until it either dissociates or absorbs a vacancy to form a V_5, which is immobile and does not dissociate on the present time and temperature scales. V_5 starts to form after ∼100 s at 220 K while all other clusters remain negligible [Fig. 4(a)]. In stage III (between 200 and 250 K), the microstructure after 2000-s annealing is composed almost exclusively of V_1 and V_5 [Fig. 4(c)]. The latter could therefore be the so far unidentified clusters measured by PAS in this temperature range.[9] At temperatures above ∼250 K, i.e. stage IV, V_2 is produced at higher rates and absorbed by either V_4 or V_5. This initiates the formation of larger clusters that may contain 100 vacancies after annealing. As shown in Fig. 4(b), pentavacancies form at the beginning of the annealing. They serve as nuclei and are replaced by larger clusters at longer times. In stage IV between ∼250 and 350 K, the microstructure contains only large clusters [Fig. 4(c)], again in agreement with PAS.[9] Finally, above 350 K (stage V), the larger clusters are unstable, dissociating down to V_1 and V_2 that are absorbed at the sink, leading to a full recovery of the system.

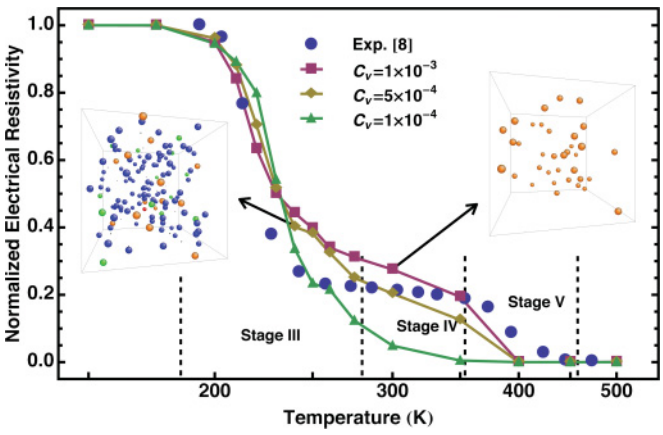

FIG. 5. (Color online) Electrical resistivity as a function of annealing temperature obtained from the present KMC simulations (with different initial vacancy concentrations) and experimental measurements from Ref. 8. The annealing time is 2000 s. Recovery stages are marked with dashed lines after Ref. 8. Insets: Simulated cluster configurations dominated by V_5 at 220 K and by V_L at 300 K. V_1: black; V_2: purple; V_3: red; V_4: green; V_5: blue; and V_L: orange.

The electrical resistivity of the simulated microstructures, evaluated using the cluster resistivities computed by Martin,[24,25] is compared in Fig. 5 to the measurements of Wampler and Gauster.[8] The simulations reproduce well the strong decrease of resistivity in stage III but less well the plateau in stage IV. We checked, however, that the resistivity in stage IV depends critically on the details on the simulations: the initial vacancy concentration as demonstrated in Fig. 5, as well as the density of sinks and the extrapolations used for the binding energy and resistivity of large clusters. Such dependence is also known experimentally,[8] where the existence of stage IV depends on the sample microstructure (single crystal or polycrystal) and the supersaturation condition (quenched or irradiated).[8] In any event, the main point here is that the early stage of clustering, stage III, where the KMC simulations were fitted on atomistic data, is well reproduced, confirming that the simulations capture the essential physics of the early stage of vacancy clustering in fcc aluminum.

In summary, we have identified a reconstructed configuration, the pentavacancy, that plays an essential role in vacancy clustering in fcc aluminum. This unexpected configuration was identified thanks to a combination of MD simulations and saddle-point searches, an approach that proved also successful for interstitial clusters in bcc iron.[7,19,26] These works show the importance of systematically exploring the potential energy landscape of small defect clusters, whether they contain vacancies or interstitials and in systems of different crystallographies, in order to identify stable reconstructed configurations that may strongly affect the kinetics of defect evolution.

We are grateful to Francois Willaime for insightful discussions. This work is supported by the French National Research Agency under project ATOPLAST and the Natural Science Foundation of China under Grant No. 50911130367.

*hao.wang@simap.grenoble-inp.fr; haowang@imr.ac.cn

†Deceased.

[1]R. W. Balluffi, S. M. Allen, and W. C. Carter, *Kinetics of Materials* (Wiley, Hoboken, NJ, 2005).

[2]R. M. J. Cotterill, M. Doyama, J. J. Jackson, and M. Meshii, *Lattice Defects in Quenched Metals* (Academic, New York, 1965).

[3]B. N. Singh, A. J. E. Foreman, and H. Trinkaus, J. Nucl. Mater. **249**, 103 (1997).

[4]M. Kiritani, Y. Satoh, Y. Kizuka, K. Arakawa, Y. Ogasawara, S. Arai, and Y. Shimomura, Philos. Mag. Lett. **79**, 797 (1999).

[5]D. J. Bacon, Y. N. Osetsky, and D. Rodney, in *Dislocations in Solids*, edited by J. P. Hirth and L. Kubin (Elsevier, Amsterdam, 2009), Chap. 88.

[6]C.-C. Fu, J. D. Torre, F. Willaime, J.-L. Bocquet, and A. Barbu, Nat. Mater. **4**, 68 (2005).

[7]Y. Fan, A. Kushima, S. Yip, and B. Yildiz, Phys. Rev. Lett. **106**, 125501 (2011).

[8]W. R. Wampler and W. B. Gauster, J. Phys. F **8**, L1 (1978).

[9]C. Szeles, Z. Kajcsos, and A. Vértes, Phys. Rev. B **31**, 1302 (1985).

[10]M. Kiritani, J. Phys. Soc. Jpn. **19**, 618 (1964).

[11]H. Wang, D. S. Xu, R. Yang, and P. Veyssière, Acta Mater. **57**, 3725 (2009).

[12]H. Wang, D. S. Xu, R. Yang, and P. Veyssière, Acta Mater. **56**, 4608 (2008).

[13]H. Wang, D. S. Xu, R. Yang, and P. Veyssière, Acta Mater. **59**, 10 (2011).

[14]G. H. Vineyard, Discuss. Faraday Soc. **31**, 7 (1961).

[15]Y. Shimomura and R. Nishiguchi, Radiat. Eff. Defects Solids **141**, 311 (1997).

[16]Y. Mishin, D. Farkas, M. J. Mehl, and D. A. Papaconstantopoulos, Phys. Rev. B **59**, 3393 (1999).

[17]B. L. Eyre, J. Phys. F **3**, 422 (1973).

[18]D. Rodney and C. Schuh, Phys. Rev. Lett. **102**, 235503 (2009).

[19]M. C. Marinica, F. Willaime, and N. Mousseau, Phys. Rev. B **83**, 094119 (2011).

[20]G. Henkelman and H. Jónsson, J. Chem. Phys. **113**, 9978 (2000).

[21]N. Soneda and T. D. de la Rubia, Philos. Mag. A **78**, 995 (1998).

[22]A. B. Bortz, M. H. Kalos, and J. L. Lebowitz, J. Comput. Phys. **17**, 10 (1975).

[23]R. O. Simmons and R. W. Balluffi, Phys. Rev. **117**, 52 (1960).

[24]J. W. Martin, J. Phys. F **2**, 842 (1972).

[25]J. W. Martin and R. Paetsch, J. Phys. F **3**, 907 (1973).

[26]D. A. Terentyev, T. P. C. Klaver, P. Olsson, M. C. Marinica, F. Willaime, C. Domain, and L. Malerba, Phys. Rev. Lett. **100**, 145503 (2008).